Chemistry & Biology
Article

Structure of *Saccharomyces cerevisiae* Chitinase 1 and Screening-Based Discovery of Potent Inhibitors

Ramon Hurtado-Guerrero[1] and Daan M.F. van Aalten[1,*]
[1] Division of Biological Chemistry & Molecular Microbiology, School of Life Sciences, University of Dundee, Dundee DD1 5EH, Scotland, UK
*Correspondence: dava@davapc1.bioch.dundee.ac.uk
DOI 10.1016/j.chembiol.2007.03.015

SUMMARY

Chitinases hydrolyse the β(1,4)-glycosidic bonds of chitin, an essential fungal cell wall component. Genetic data on a subclass of fungal family 18 chitinases have suggested a role in cell wall morphology. Specific inhibitors of these enzymes would be useful as tools to study their role in cell wall morphogenesis and could possess antifungal properties. Here, we describe the crystallographic structure of a fungal "plant-type" family 18 chitinase, that of *Saccharomyces cerevisiae* CTS1. The enzyme is active against 4-methylumbelliferyl chitooligosaccharides and displays an unusually low pH optimum for activity. A library screen against *Sc*CTS1 yielded hits with K_i's as low as 3.2 μM. Crystal structures of *Sc*CTS1 in complex with inhibitors from three series reveal striking mimicry of carbohydrate substrate by small aromatic moieties and a pocket that could be further exploited in optimization of these inhibitors.

INTRODUCTION

Chitin is a tough, rigid, protective, linear polymer of β(1,4)-*N*-acetyl-D-glucosamine (GlcNAc) and is a component of arthropod exoskeletons and the cell walls of fungi. In these organisms a dynamic balance between chitin synthesis (through chitin synthases) and chitin hydrolysis (through chitinases) is required to allow for growth and morphogenesis [1]. Chitinases, the enzymes that catalyze the hydrolysis of the β(1,4)-glycosidic bonds between GlcNAc monomers, belong to CAZY (http://afmb.cnrs-mrs.fr/CAZY) [2] glycoside hydrolase family 18 or 19. Fungi belonging to the phylum Ascomycota possess several family 18 chitinases belonging to two subclasses—some of these enzymes are similar to the well-characterized plant chitinase hevamine from *Hevea brasiliensis* [3–5] (the "plant-type" family 18 chitinases), whereas others are similar to the chitinases first characterized in bacteria ("bacterial-type" family 18 chitinases) [6]. For instance, *Saccharomyces cerevisiae* possesses two chitinase-encoding genes: the plant-type chitinase *Sc*CTS1 [7] with an apparent molecular weight of 130 kDa (including glycosylation) showing sequence similarity to hevamine; and *Sc*CTS2 [8], which is more similar to bacterial chitinases like chitinase A and B from *Serratia marcescens* [6]. The genomes of the fungal pathogens *Aspergillus fumigatus* and *Candida albicans* contain many chitinases, with the former containing 14 chitinases (of which 5 are of the plant-type [9]) and the latter 4 (of which 3 are of the plant-type [10]).

The bacterial-type chitinases have been extensively studied. These enzymes are generally believed to show mainly exo-activity, i.e., removing short chitooligosaccharides from the end of long chitin chains [6]. Structures for several of these enzymes, including chitinases A and B from *S. marcescens* [11, 12] and several fungal chitinases [13, 14] and mammalian chitinases [15], have been reported, revealing a conserved catalytic core with several exposed aromatic residues that are important for substrate binding (Figure 1). Gene disruption studies of the bacterial-type chitinase genes in *A. fumigatus* and *Coccidioides immitis* have not revealed any significant phenotype, and it has been suggested that this subclass of family 18 chitinases plays a role in metabolizing short exogenous chitooligosaccharides [16, 17]. In contrast, observable phenotypes have been reported for the disruption of plant-type chitinases in fungi. A knockout of the *cts1* gene in *S. cerevisiae* resulted in a "clumping" phenotype, where, after cell division, mother and daughter cells were unable to separate [18]. Treatment of *S. cerevisiae* with a derivative of allosamidin (a well-characterized chitinase inhibitor [19]) gave a remarkably similar phenotype [20]. Furthermore, disruption of the *chiA* gene in *A. nidulans* resulted in reduced germination and hyphal growth [21]. Deletion of chitinase 3 from *C. albicans* generated elongated chains of unseparated cells in the yeast growth phase, resembling the phenotype of *S. cerevisiae cts1* knockouts [10].

Despite the key role these plant-type chitinases appear to play in fungal cell wall morphology and biogenesis, they have not been extensively characterized. *Sc*CTS1 is divided into four domains [18]: a signal sequence (amino acids 1–20), a catalytic domain (amino acids 21–315), a Ser/Thr-rich domain (amino acids 315–480), and a high-affinity chitin-binding domain (amino acids 481–562). This domain organization is similar to most of the plant-type chitinases in *A. fumigatus* and *C. albicans*

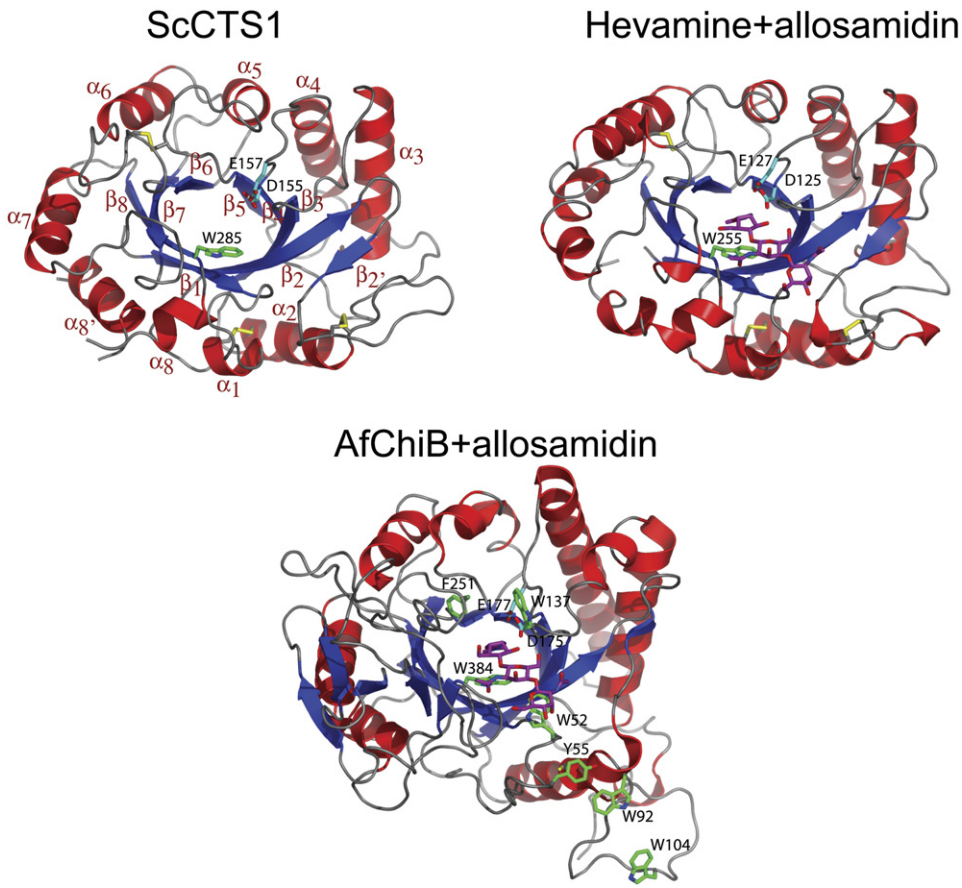

Figure 1. Overall Structure of *Sc*CTS1 and Comparison to Other Family 18 Chitinases

Native *Sc*CTS1 structure compared to the hevamine-allosamidin (PDB code 1LLO [23]) and *Af*ChiB-allosamidin (PDB code 2A3E [14]) complexes. The Glu157 and Asp155 from the family 18 chitinase DxE motif are shown with cyan carbon atoms (the equivalent residues in hevamine and *Af*ChiB are shown with the same colors). The three disulphide bridges in *Sc*CTS1 and hevamine are represented in yellow. Solvent-exposed aromatic residues are shown with green carbon atoms. Allosamidin is shown with magenta carbon atoms.

[9, 10]. The chitin-binding domain of *Sc*CTS1 may have a role in localizing the enzyme to the cell wall [18]. Perhaps due to their size, domain organization, or membrane localization, only a few plant-type fungal chitinases have so far been successfully overproduced in recombinant form (e.g., [22]). However, hevamine, the plant chitinase from *H. brasiliensis*, has been characterized in some detail. Hevamine has been shown to be an endo-chitinase [3, 5] with a catalytic core distantly similar to those of the bacterial-type chitinases, but possessing a more exposed substrate-binding groove. Structural work on hevamine in conjunction with inhibitor studies was instrumental in showing that this enzyme, and indeed all family 18 chitinases, proceed through a ''substrate-assisted'' reaction mechanism where the *N*-acetyl moiety of the sugar toward the nonreducing end of the glycosidic bond acts as a nucleophile, forming an oxazolinium ion intermediate [3, 23, 24]. The potent chitinase inhibitor allosamidin, a pseudotrisaccharide [19, 25], accurately mimics this reaction intermediate, as elegantly shown through X-ray crystallographic studies [23], and inhibits most chitinases from the GH 18 family. Mutagenesis studies on hevamine have confirmed the role of the two acids in the conserved GH 18 DxE motif, with the glutamate being the catalytic acid protonating the glycosidic bond, and the aspartate playing a key role in assisting the acetamido group in its nucleophilic attack and stabilizing the developing positive charge on the oxazolinium ion [5, 24].

Despite the considerable amount of genetic data on the fungal plant-type chitinases, their precise roles are still unclear. This is largely due to the presence of many of these genes in the fungal genomes and the shortcomings of the genetic approach in terms of generating multiple-gene knockouts to overcome the effects of redundancy. Given the relatively large degree of sequence conservation of these enzymes, it is possible that a potent, specific, small-molecule inhibitor could be developed that would inhibit all plant-type chitinases, allowing the phenotype of a total knockdown of these enzymes to be studied. Furthermore, such a molecule could be a lead for the development of a chitinase inhibitor with antifungal properties.

Here, we have taken a first step in this direction by developing an overexpression system for *Sc*CTS1 and determining its structure by X-ray crystallography. A

Table 1. Details of Data Collection and Structure Refinement

	Native	8-Chlorotheophylline	Kinetin	Acetazolamide
Unit cell (Å)	a = 73.63	a = 73.41	a = 73.34	a = 73.44
	b = 112.83	b = 112.71	b = 111.62	b = 113.51
	c = 37.35	c = 37.33	c = 37.26	c = 37.49
Resolution (Å)	20–1.60 (1.66–1.60)	20–1.90 (1.97–1.90)	20–1.60 (1.66–1.60)	20–1.75 (1.81–1.75)
# Observed reflections	135,336 (11,786)	84,124 (8,133)	141,115 (9,208)	122,213 (11,354)
# Unique reflections	39,503 (3,745)	24,548 (2,419)	39,904 (3,162)	30,667 (3,049)
Redundancy	3.4 (3.1)	3.4 (3.4)	3.5 (2.9)	4.0 (3.7)
I/σI	14.9 (3.3)	9.0 (3.0)	9.7 (2.3)	9.4 (2.4)
Completeness	94.2 (90.8)	98.3 (98.8)	96.8 (78.1)	95.4 (96.9)
R_{merge}	0.036 (0.285)	0.081 (0.434)	0.078 (0.390)	0.072 (0.433)
R, R_{free}	0.166, 0.192	0.198, 0.258	0.193, 0.222	0.183, 0.232
Rmsd from ideal geometry				
Bonds (Å)	0.014	0.016	0.014	0.014
Angles (°)	1.4	1.5	1.5	1.5
B factor rmsd (Å^2) (backbone bonds)	0.83	0.86	0.81	0.83
<B > (Å^2)				
Protein	20.1	12.9	27.1	33.2
Ligand	36.9	9.1	19.0	36.8
Water	28.5	18.0	29.7	33.7

Values in parentheses are for the highest resolution shell. All measured data were included in structure refinement. All crystals were of space group $P2_12_12$.

high-throughput screen based on a fluorescent enzyme assay was then used to identify three inhibitor scaffolds. The most potent of these, kinetin ($K_i = 3.2\ \mu M$), is a competitive inhibitor of the enzyme that occupies a deep pocket. Site-directed mutagenesis was used to reveal the importance of this pocket in determining inhibitor potency. This work provides a solid basis for the development of a plant-type fungal chitinase inhibitor.

RESULTS AND DISCUSSION

*Sc*CTS1 Contains a Substrate-Binding Groove Compatible with Endo Activity

Characterization of the activity and structure of the "plant-type" fungal chitinases has been hampered by difficulties in overexpressing recombinant forms of these enzymes. We have expressed the catalytic domain of *Sc*CTS1 (comprising of amino acids 22 to 315) as a secreted N-terminally His-tagged fusion protein in *Pichia pastoris*, producing approximately 50 mg per liter of medium. Purification using Ni-affinity chromatography and gel filtration yielded approximately 15 mg of pure protein per liter of media. The protein was then crystallized from phosphate buffers, and the structure was solved by molecular replacement and refined against synchrotron diffraction data to 1.6 Å (Table 1).

The *Sc*CTS1 structure represents the first example, to our knowledge, of a plant-type fungal chitinase. The nearest structural homolog is the plant chitinase hevamine [3], which is 36% identical at the sequence level and superposes onto *Sc*CTS1 with an rmsd of 1.6 Å on 256 Cα atoms (Figure 1). The typical $(\beta/\alpha)_8$ TIM-barrel is structurally conserved, as are the three disulphide bonds (Figure 1).

Although the active site residues and TIM-barrel fold are conserved, there exist significant structural differences between *Sc*CTS1 and the bacterial-type fungal chitinase, as evident from a comparison with the *A. fumigatus* chitinase B1 (*Af*ChiB1) structure [14] (Figure 1). Most notable is the fact that, whereas *Sc*CTS1 and hevamine contain a minimal TIM-barrel fold similar to the structure of TinyTIM [26], *Af*ChiB1 contains a highly decorated TIM-barrel with a large α/β domain inserted in one of the loops and several other larger loops (Figure 1). The result of this is that, whereas *Sc*CTS1 and hevamine contain a shallow substrate-binding groove, the bacterial-type chitinases contain deep substrate-binding grooves, in some cases even forming tunnels [11–15, 27]. There are further significant differences in the nature of the side chains lining the substrate-binding grooves. Whereas a large path of highly conserved aromatic residues involved in substrate binding lines the active-site grooves of the bacterial-type chitinases [15, 27, 28], there is only one conserved solvent-exposed tryptophan in *Sc*CTS1 (Trp285) and hevamine (Trp255) (Figure 1). This difference in substrate-binding groove architecture correlates with the known endo-chitinase activities of *Sc*CTS1 [7] and hevamine [4] and the mostly exo-acting bacterial-type chitinases [6].

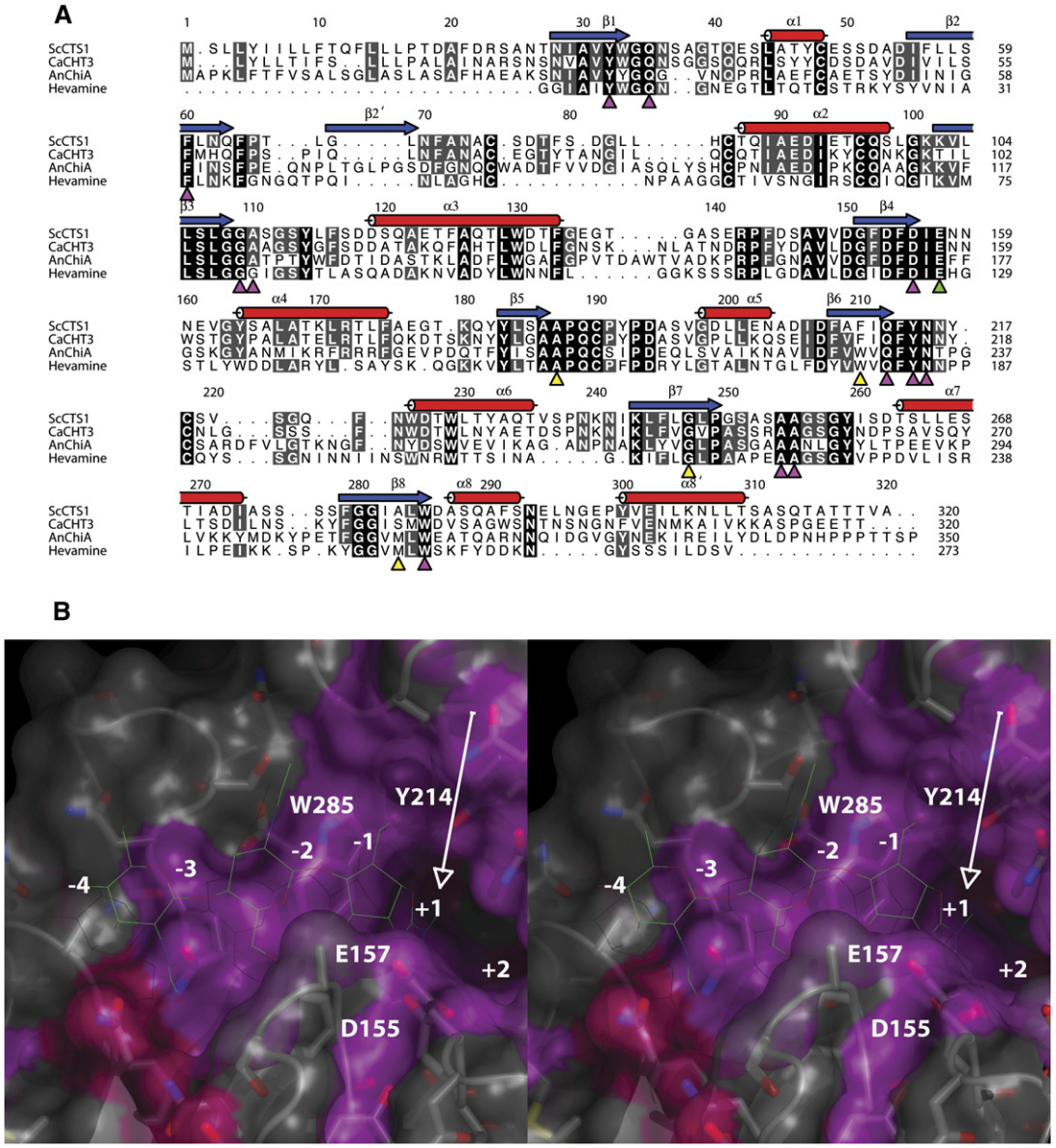

Figure 2. Sequence Conservation in the Plant-Type Fungal Family 18 Chitinases

(A) Multiple sequence alignment between the catalytic cores of *Sc*CTS1, *Ca*CHT3, *An*ChiA, and hevamine. Green triangles represent the catalytic glutamic acids, pink triangles identify active site residues, and yellow triangles represent amino acids in a plant-type family 18 chitinase specific pocket.

(B) Stereo image of the native *Sc*CTS1 structure, with a molecular surface colored by sequence conservation following the alignment in (A) (magenta = identical residue, pink = conserved residue, gray = unconserved residue). Allosamidin (thin lines) from the hevamine-allosamidin complex is superposed into the *Sc*CTS1 active site for reference. The −4 to +2 sugar-binding subsites following standard nomenclature are labeled. The arrow indicates the pocket referred to in (A).

The Plant-Type Fungal Chitinases Possess a Conserved Active Site

Previous structural studies of hevamine in complex with the inhibitor allosamidin [23] (Figures 1 and 2B) or substrate fragments [3, 24] have defined the GlcNAc subsites in the enzyme, which form a shallow groove on the surface of the protein, also observed in the *Sc*CTS1 structure (Figure 2B). The groove consists of six sugar-binding subsites, numbered from −4 (the nonreducing end) to +2 (the reducing end), with hydrolysis taking place on the glycosidic bond between the −1 and +1 subsites [3, 23, 24]. Subsites −4 and −3 are highly solvent exposed, and the side chains forming these subsites are not well conserved (Figures 2A and 2B). Subsites −2 to +2 form a deep groove, lined by side chains that are highly conserved in the plant-type family 18 chitinases (Figures 2A and 2B).

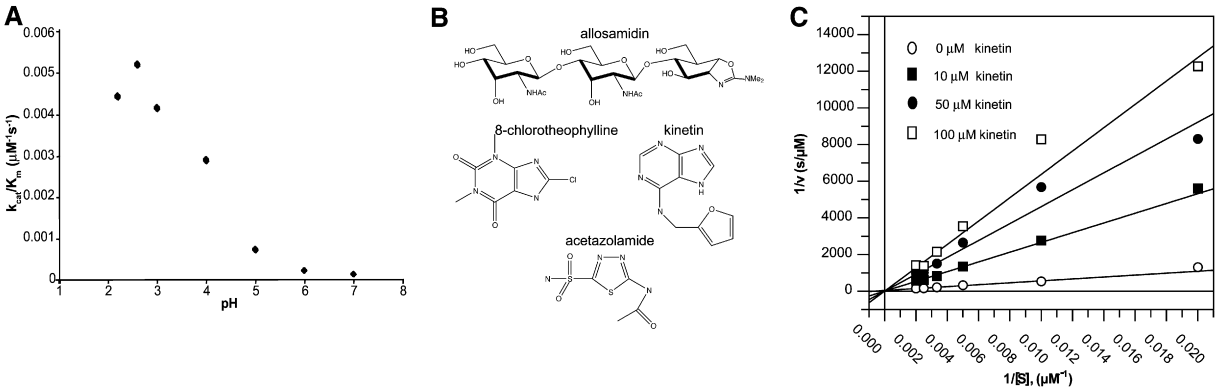

Figure 3. Enzyme Activity and Inhibition

(A) pH-activity profile of k_{cat}/K_m at different concentrations of substrate (4MU-$GlcNAc_3$) (from 0 to 800 μM) for *Sc*CTS1.

(B) Chemical structures of allosamidin, 8-chlorotheophylline, acetazolamide, and kinetin.

(C) Lineweaver-Burk plots of kinetin measured against *Sc*CTS1 at different concentrations of inhibitor. A fit of all the data against a competitive inhibition model resulted in a K_i of 3.2 ± 0.3 μM, with a V_{max} of 0.0066 ± 0.0015 μM/s and K_m of 1000 ± 30 μM.

In the −1 subsite, Asp155 and Glu157 in *Sc*CTS1 (equivalent to Asp125 and Glu127 in hevamine) at the end of β4 correspond to the residues in the family 18 chitinase DxE motif (see CAZY [2]). Glu157 is the catalytic acid, with Asp155 stabilizing the oxazolinium ring of the reaction intermediate. Notably, a tryptophan that is completely conserved in all family 18 chitinases (Trp285 in *ScCTS1*, equivalent to Trp255 in hevamine) forms the bottom of the −1 subsite, with a conserved tyrosine (Tyr214 in *ScCTS1*, equivalent to Tyr183 in hevamine) forming one of the sides. The −2 and −3 subsites are considerably more exposed; nevertheless, most of the residues that are seen to hydrogen bond the −2/−3 sugars in the hevamine-allosamidin complex are also conserved in *Sc*CTS1 [23] (Figure 2B). In the *Sc*CTS1 structure, a pocket lined with conserved residues is observed next to the −1 subsite (Figures 2A and 2B).

Recombinant *Sc*CTS1 Is Active against 4MU-Glycosides

The activities of *Sc*CTS1 and hevamine on polymeric chitin have been extensively studied, showing that these enzymes are endo-chitinases [3, 5, 7]. To allow future rapid evaluation of inhibitors, we decided to investigate the activity of *Sc*CTS1 on 4-methylumbelliferyl chitooligosaccharides. Steady-state kinetics of *Sc*CTS1 was established with 4MU-$GlcNAc_3$, yielding a K_m of 1 mM, with a k_{cat} of 1.3 s^{-1}. While the turnover rate of the enzyme is comparable to the steady kinetics reported for hevamine on $GlcNAc_5$, there exists a significant difference in the K_m (K_m of 16 μM, with a k_{cat} of 0.6 s^{-1} for hevamine [5]). This difference is likely to be due to the degree of polymerization of the substrate and the presence of the 4MU group instead of a GlcNAc unit in the +1 subsite. Activity against 4MU-$GlcNAc_2$ was also tested, and although turnover could be detected this was not sufficient to establish proper steady-state kinetics.

Recombinant *Sc*CTS1 Has an Unusual pH Optimum

Using the 4MU-$GlcNAc_3$ substrate, the pH dependence of *Sc*CTS1 in the pH range 2.2–7.0 was investigated. The enzyme shows a significant increase in activity toward the low pH range, with maximal k_{cat} of 5.7 s^{-1} and k_{cat}/K_m of 0.0052 $s^{-1}\mu M^{-1}$ at pH 2.6 (Figure 3A). The K_m in the pH 2.2–5.0 range was between 1.0 and 1.4 mM, while at pH 6 and 7 the K_m was 3.0 and 2.8 mM, respectively. This is similar to what has been described for native *Sc*CTS1 partially purified from yeast extracts [7] and hevamine [5]. Such an unusual pH optimum has not been observed for the bacterial-type chitinases, which generally possess pH optima around pH 5–6 [6], with one notable exception. The acid mammalian chitinase (AMCase), which falls within the bacterial-type chitinase subclass, also displays a pH optimum of around 2–3 [29]. Recent structural analysis of human AMCase has revealed that this shift in pH optimum is due to the mutation of a basic residue adjacent to a conserved aspartic acid positioned near the substrate in the −1 subsite of the active site (O.A. Andersen and D.M.F.v.A., unpublished data). Interestingly, in all plant-type family 18 chitinases this conserved aspartic acid is changed to a conserved asparagine (Asn215 in *Sc*CTS1; Figure 2A). Mutation of the aspartic acid to an alanine in the bacterial-type family 18 chitinase B from *S. marcescens* resulted in a significant downward shift of the pH optimum [30]. It is tempting to speculate that the asparagine at the equivalent position in the plant-type fungal chitinases is the source of the unusually low pH optimum.

*Sc*CTS1 Is Inhibited by Allosamidin and Purine Derivatives

Allosamidin is a potent inhibitor of both bacterial-type and plant-type family 18 chitinases, and its mode of binding has been extensively characterized through enzymology and X-ray crystallography [13, 14, 23, 27, 31]. The hevamine-allosamidin complex has shown that the inhibitor

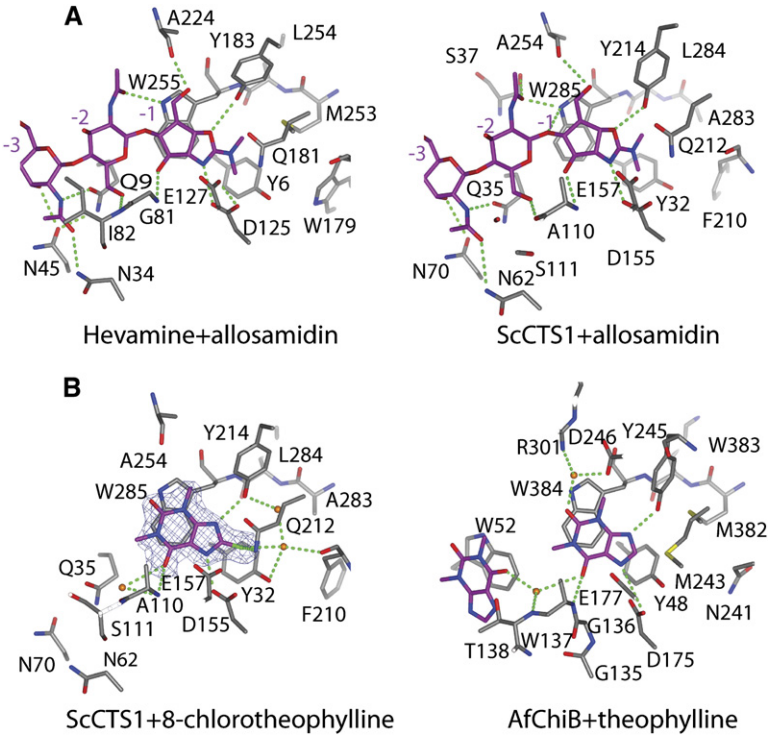

Figure 4. Comparison of Allosamidin and Theophylline Binding to Family 18 Chitinases

(A and B) Comparison of hevamine in complex with allosamidin (PDB entry 1LLO [23]), with a model of *Sc*CTS1 in complex with allosamidin, obtained by superposition of the hevamine-allosamidin complex (A), and comparison of *Sc*CTS1 in complex with 8-chlorotheophylline and the previously determined *Af*ChiB-theophylline complex [33] (B). Residues lining the active site are shown as sticks with gray carbon atoms. Inhibitors are shown as sticks with magenta carbon atoms. Protein-inhibitor hydrogen bonds are shown as dotted green lines. Unbiased (i.e., before inclusion of any inhibitor model) $|F_o| - |F_c|$, f_{calc} electron density maps are shown at 2.5σ. In the allosamidin complexes, the sugar subsites are labeled from −3 to −1. Water molecules involved in hydrogen bonds with the ligand or the protein are shown as orange spheres.

mimics the oxazolinium intermediate through hydrogen bonds with the conserved Asp125 (Asp155 in *Sc*CTS1) and Tyr183 (Tyr214 in *Sc*CTS1) and extensive stacking with the conserved Trp255 (Trp285 in *Sc*CTS1) [23] (Figure 4). A modeled *Sc*CTS1-allosamidin complex shows that the majority of the hydrogen bond interactions between the enzymes and the two sugars are conserved (Figure 4A). Given the conservation of these residues throughout the plant-type fungal chitinases, it is not surprising that allosamidin has been reported to inhibit partially purified *Sc*CTS1 [20]. Similarly the *Sc*CTS1 recombinant enzyme is competitively inhibited by allosamidin (K_i = 0.61 ± 0.02 μM [Table 2]; the K_i against hevamine has been reported to be 3.1 μM [4]). Allosamidin is not an attractive starting point for the synthesis of potent plant-type fungal chitinase inhibitors due to its inherent non-drug-likeness (hydrophilic cLogP [−5.2], high molecular weight, and presence of glycosidic bonds) and its complicated synthesis [32]. Recently, the more drug-like purine theophylline and derivatives thereof were identified as competitive bacterial-type family 18 chitinase inhibitors, displaying up to 3 μM inhibition and extensive mimicry of the allosamidin-chitinase interactions, as shown in Figure 4B [33, 34]. We investigated the inhibitory potential of these compounds against *Sc*CTS1, revealing that the theophylline derivative 8-chlorotheophylline inhibits the enzyme with a K_i of 600 ± 64 μM (Table 2). This prompted us to investigate the binding mode of this compound. The crystal structure of *Sc*CTS1 complexed with 8-chlorotheophylline was determined to 1.9 Å, with the final model of the complex giving an R factor of 0.198 (R_{free} = 0.258). The inhibitor shows extensive π-π stacking with Trp285 in the bottom of the −1 subsite, occupying the same position as observed in the *Af*ChiB-theophylline complex (Figure 4). Furthermore, the same hydrogen bonds are observed, from Tyr214 to the N9 nitrogen, from Asp155 to the N7 nitrogen, and from the backbone nitrogen of Ala110 to the O6 oxygen of the inhibitor. Notably, the 8-chloro atom points into the direction of the deep pocket that is observed in the native *Sc*CTS1 structure (Figure 2B)—this pocket is absent in the structure of bacterial-type chitinases such as *Af*ChiB1 (Figure 4B). Strikingly, two water molecules are occupying this pocket in the *Sc*CTS1-8-chlorotheophylline complex (Figure 4B). This suggests that inhibitors possessing moieties that could occupy this pocket and displace these water molecules would give additional favorable entropic contributions to binding.

Table 2. Inhibition of Wild-Type *Sc*CTS1, the Ala283Ser Mutant, and the Ala283Ser/Phe210Trp Double Mutant by Allosamidin, Kinetin, Acetazolamide, and 8-Chlorotheophylline

	WT	Ala283Ser	Ala283Ser/ Phe210Trp
Allosamidin	0.61 ± 0.02	0.66 ± 0.4	1.46 ± 0.03
Kinetin	3.2 ± 0.3	>5000	>5000
Acetazolamide	21 ± 2	71 ± 17	128 ± 11
8-Chlorotheophylline	600 ± 64	1155 ± 87	1192 ± 262

The values shown are K_is in μM, calculated from Lineweaver-Burk analysis (for kinetin and acetazolamide against WT) or from IC_{50} curves using the Cheng & Prusoff equation (all other values). Errors represent standard deviation.

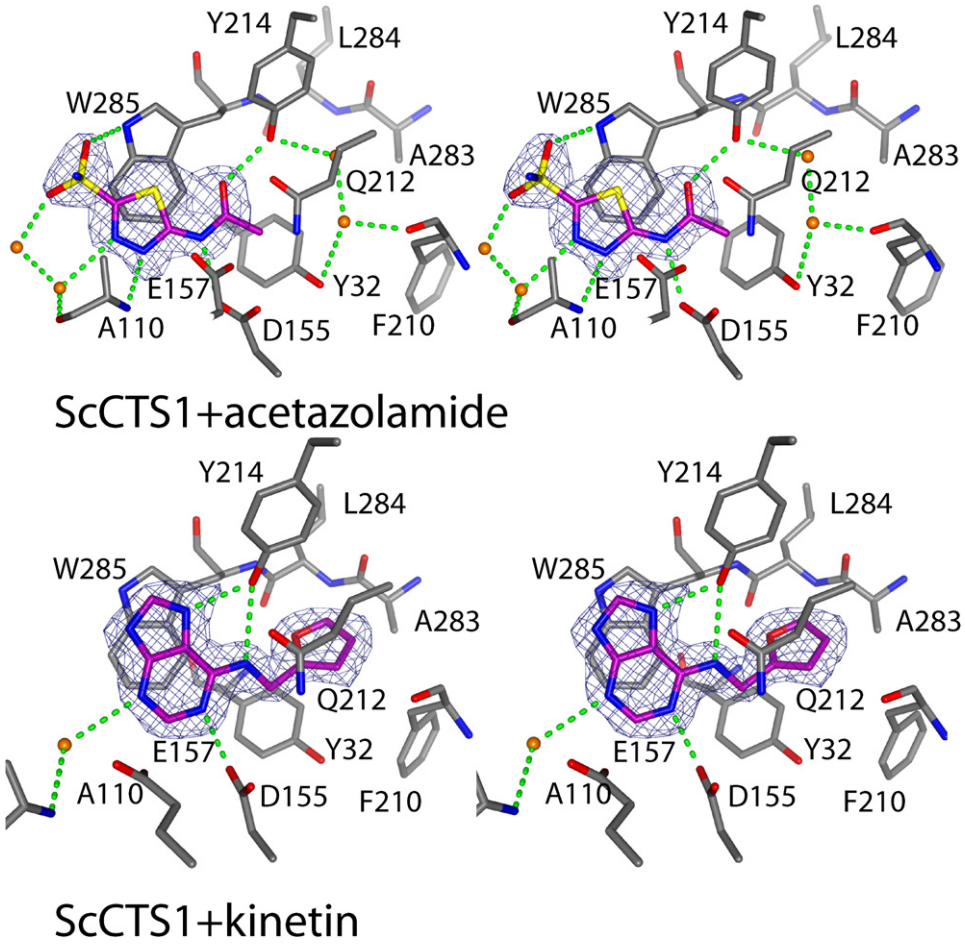

Figure 5. Binding the Kinetin and Acetazolamide Inhibitors to *Sc*CTS1

The structures of the *Sc*CTS1-kinetin and *Sc*CTS1-acetazolamide complexes are shown. Residues lining the active site are shown as sticks with gray carbon atoms. Inhibitors are shown as sticks with magenta carbon atoms. Protein-inhibitor hydrogen bonds are shown as dotted green lines. Unbiased (i.e., before inclusion of any inhibitor model) $|F_o| - |F_c|$, f_{calc} electron density maps are shown at 2.5σ. Water molecules involved in hydrogen bonds with the ligand or the protein are shown as orange spheres.

We next attempted to identify such inhibitors by a high-throughput screening campaign using a library of drug molecules.

Discovery of *Sc*CTS1 Inhibitors Kinetin and Acetazolamide

A library of 880 drug-like molecules (The Prestwick Chemical Library) was screened at 40 μg/ml (approximately equivalent to 80 μM, assuming a molecular weight of 500) using 100 μM of 4MU-$GlcNAc_3$. This led to the identification of two structurally distinct inhibitors, kinetin (a plant hormone) and acetazolamide (a well known carbonic anhydrase inhibitor) (Figure 3B). We next investigated the mode of inhibition of these compounds. Steady-state kinetics at different concentrations of 4MU-$GlcNAc_3$ in the presence of increasing amounts of the inhibitors showed that kinetin (K_i = 3.2 μM; Figure 3C) and acetazolamide (K_i = 21 μM) were both competitive inhibitors.

Next, the binding modes of these inhibitors were investigated by X-ray crystallographic analysis of their complexes with *Sc*CTS1. The *Sc*CTS1-acetazolamide complex was refined against 1.75 Å synchrotron data, yielding a final model with an R factor of 0.183 (R_{free} = 0.232; Table 1). Despite containing a substantially different aromatic heterocycle, acetazolamide binds in a surprisingly similar mode as 8-chlorotheophylline (Figures 4B and 5). The stacking interaction with Trp285, and the hydrogen bonds with Tyr214, Asp155, and the backbone of Ala110 are conserved.

An additional hydrogen bond is observed between the catalytic acid (Glu157) and the acetamido nitrogen (Figure 5). The sulfonamide group points toward the −2/−3 subsites, making weak interactions with the Trp285 indole nitrogen and an ordered water molecule. Notable, the deep pocket present in the *Sc*CTS1 structure is still occupied by two ordered water molecules (Figure 5).

The structure of the *Sc*CTS1-kinetin complex was refined against 1.6 Å synchrotron data, yielding a final model with an R factor of 0.193 (R_{free} = 0.222; Table 1). Although the purine substructure of kinetin binds in the same

position as 8-chlorotheophylline, it does so in a different orientation (Figures 4 and 5). There is still extensive stacking between the purine moiety and Trp285, and hydrogen bonds to Tyr214 and Asp155 are also observed. The direct hydrogen bond to the backbone nitrogen of Ala110 observed in the 8-chlorotheophylline and acetazolamide complexes is a water-mediated hydrogen bond in the kinetin complex (Figures 4 and 5). However, the main difference between the binding mode of kinetin and the other previously characterized inhibitors is that the kinetin furan group occupies the deep pocket, displacing the previously observed ordered water molecules in the 8-chlorotheophylline/acetazolamide complexes (Figures 4 and 5). Furthermore, the furan group oxygen is also in a position suitable for stacking with the Tyr32 aromatic side chain. These extra interactions of the furfuryl group are likely to be the source of the tighter binding of the inhibitor, approaching the inhibition by allosamidin to within an order of magnitude.

A Key Amino Acid Regulates Plant-Type Fungal Chitinase Inhibitor Sensitivity

The deep pocket in the *Sc*CTS1 chitinase (Figures 2B, 4, and 5) appears to be a key opportunity for increasing affinity both through displacement of ordered water molecules and establishment of further interactions. However, while the catalytic machinery of the plant-type fungal chitinases is fully conserved, analysis of sequence conservation around this pocket reveals two positions of sequence variation (Figure 2). Amino acid 283 is an alanine, situated at the bottom of the *Sc*CTS1 pocket (Figure 4). In hevamine, however, this residue is a much larger methionine (Met253; Figure 4A). A methionine is also observed in *A. nidulans* chitinase A, whereas a serine is present at the equivalent position in all *C. albicans* plant-type chitinases (Figure 2). It is thus worth establishing the effect of the presence of these larger side chains on the inhibitory potential of the inhibitors studied here. The *Sc*CTS1 mutant A283S was made, emulating the pocket as present in the *C. albicans* plant-type chitinases. Steady-state kinetics of this mutant showed a similar K_m (0.8 versus 1 mM for wild-type) and turnover number k_{cat} (2.3 versus 1.3 for wild-type) as for the wild-type enzyme. Strikingly, while inhibition by allosamidin, acetazolamide, and 8-chlorotheophylline (Table 2) appeared to not be significantly affected by the larger serine present at position 283, inhibition by kinetin was no longer detectable. These data indicate that while in the *C. albicans* plant-type chitinases, which possess the large serine, a pocket may still exist, it is no longer able to accommodate large groups such as the kinetin furan side chain. It is likely that the methionines observed at this position for both the *A. nidulans* chitinase A and hevamine (Figure 2) would similarly abolish inhibition by kinetin. Indeed, the presence of this methionine in hevamine could be the source of the difference in allosamidin inhibition of *Sc*CTS1 (K_i = 0.61 μM) and hevamine (K_i = 3.1 μM).

The second position of sequence variation in the pocket in *Sc*CTS1 is Phe210, which is a tryptophan in hevamine and *A. nidulans* ChiA (Figure 2). To probe the effect of this sequence variation on the structure of the pocket and binding of the inhibitors, the double mutant Phe210Trp/Ala283Ser was studied. Steady-state kinetics of this double mutant showed a similar K_m (1.1 versus 1 mM for wild-type) and turnover number k_{cat} (0.8 versus 1.3 for wild-type) as for the wild-type enzyme and the single Ala283Ser mutant. Again, while inhibition by allosamidin, acetazolamide, and 8-chlorotheophylline (Table 2) did not appear to be significantly affected by the larger Ser183 and Trp210, inhibition by kinetin was no longer detectable. These results indicate that sequence variation at position 283 appears to be a key determinant for binding affinities for inhibitors that occupy the deep pocket.

Concluding Remarks

Since the first report of the cell-clumping phenotype observed upon disruption of the *cts1* gene [18] or inhibition of the *Sc*CTS1 chitinase activity with allosamidin [20], no complete knockout of all fungal plant-type chitinases in a single organism has been reported. Due to the large amount of redundancy in the fungal chitinase genes, the genetic approach toward knocking out all chitinase activity in a single fungal species is difficult to achieve. Because of this lack of genetic data, it is still difficult to ascertain the involvement of these plant-type fungal chitinases in virulence, morphogenesis, or growth. The work described here represents a first step toward the design and synthesis of a chemical tool to give significant inhibition of this subclass of family 18 chitinases. While the three scaffolds identified do not currently give submicromolar inhibition and the most potent of these, kinetin, appears sensitive to the identity of an unconserved amino acid, they are drug-like fragments that are synthetically accessible and could be further optimized using the structural data presented here.

SIGNIFICANCE

Chitinases are enzymes that catalyze the hydrolysis of the β(1,4)-glycosidic bonds between the *N*-acetyl-D-glucosamine (GlcNAc) monomers of chitin. Within the family 18 chitinases, two subfamilies exist, the extensively studied bacterial-type chitinases and the less well-studied plant-type chitinases with as prototype hevamine from *Hevea brasiliensis*. Both classes of enzymes are found in the genomes of yeast and fungi. Whereas the bacterial-type family 18 chitinases are nonessential, genetic data on the plant-type family 18 chitinases point to a role in cell wall morphology. For example, disruption of *Aspergillus nidulans chiA* leads to a defect in germination and hyphal growth, whereas the *Saccharomyces cerevisiae* chitinase 1 (*Sc*CTS1) plays a key role in separation of mother and daughter cells at the end of cell division. Specific inhibitors of these enzymes would be useful as tools to study their role in cell wall morphogenesis and could possess antifungal properties. Here, we describe the

crystallographic structure of a fungal plant-type family 18 chitinase, that of *Sc*CTS1 and the results from a high-throughput screen against *Sc*CTS1 using a library of currently marketed drugs, which could form the basis for development of inhibitors specific for this subclass of family 18 chitinases.

EXPERIMENTAL PROCEDURES

Materials

Oligonucleotides were supplied by the oligo synthesis service (School of Life Sciences, University of Dundee, UK). Restriction enzymes were obtained from New England Biolabs. Platinum high-fidelity Taq DNA polymerase, pCR2.1TOPO, pPICZαA, and X-33 strain were from Invitrogen. 4-methylumbelliferyl-b-D-*N,N′,N″*-triacetyl-chitotrioside (4MU-$GlcNAc_3$) was from Sigma-Aldrich. HiTrapTM chelating HP column and glutathione sepharoseTM 4B were from Amersham Biosciences. All plasmids were verified by the sequencing service (School of Life Sciences, University of Dundee).

Cloning, Expression, and Purification

The *cts1* gene from *Saccharomyces cerevisiae* was amplified using Platinum Taq DNA polymerase (Invitrogen), genomic DNA (AY925), and 5′ and 3′ end primers. The forward primer was 5′-TCTTCTGGT**CTGGAAGTTCTGTTCCA**AGGGCCACTGGATAGGTCTGCTAACAC AAATATTGCTG-3′, and the reverse primer was 5′-*CCGCGG*TCAT CAGGCGGTCTGGCTAGCACTTG-3′. In the forward primer, the sequence encoding a PreScission cleavage site is shown in bold, and in the reverse primer a SacII restriction site is shown in italics. The PCR product was purified and used as a template for PCR using the 5′ end primer 5′*CTCGAG*AAAAGAGAGGCTGAAGCT**CATCACCATC ACCATCAC**TCTTCTGGTCTGAAGTTCTGTTCCAAGGGCCACTG-3′. In this primer, the sequence encoding a histidine tag is shown in bold, and a XhoI restriction site is shown in italics. The PCR product was ligated into a pCR2.1TOPO expression vector by the TOPO directional cloning procedure (Invitrogen). This vector was double digested with XhoI and SacII restriction enzymes, and the insert was ligated into pPICZαA. The plasmids were isolated from *E. coli* DH5α strain (pPICZαAsccts1). pPICZαAsccts1 was digested with SacI and transformed into X-33 strain with the LiCl method (Invitrogen). Transformants were selected on YPD plates (1% [w/v] yeast extract, 2% [w/v] peptone, 2% [w/v] dextrose) containing 100 μg/ml of zeocin (Invitrogen). Batch cultures were performed in 100 ml volume of BMGY medium (1% [w/v] yeast extract, 2% [w/v] peptone, 100 mM potassium phosphate [pH 6.0], 1.34% [w/v] yeast nitrogen base, and 1% [v/v] glycerol). 50 ml was utilized to grow 500 ml of BMGY medium overnight at 30°C, and expression was induced by methanol (1%, v/v) for 72 hr at room temperature in a shaking incubator (270 rpm). Yeast cells were harvested by centrifugation at 3480 × g for 30 min.

The supernatant of the centrifugation containing soluble *Sc*CTS1 was filtered, concentrated, and dialyzed three times against 5 liters of buffer A (50 mM sodium phosphate, 300 mM sodium chloride, and 10 mM imidazole [pH 8]) at 4°C overnight, and applied onto a HiTrap chelating HP column (5 ml) previously equilibrated with buffer A at a flow rate of 1 ml/min. The protein was washed with buffer A and eluted with buffer B (50 mM sodium phosphate, 300 mM sodium chloride, and 300 mM imidazole [pH 8]). After concentrating and dialyzing it against buffer C (50 mM HEPES, 250 mM sodium chloride, and 2 mM DTT [pH 7.5]), the protein was digested overnight with GST-PreScission protease at 4°C. The GST-PreScission protease was removed with glutathione sepharose 4B, and *Sc*CTS1 was then applied onto a gel filtration column previously equilibrated with buffer C. Protein was concentrated and analyzed by SDS-PAGE followed by Coomassie blue staining. The purified *Sc*CTS1 protein was used for kinetic analyses and crystallization trials. Construction of the *Sc*CTS1 mutants was done by mutagenesis using the QuikChange Site-Directed Mutagenesis Kit, following the manufacturer's instructions. The mutant proteins were purified using the same procedures as used for the wild-type enzyme.

Enzymology

Michaelis-Menten parameters of *Sc*CTS1 were determined using the fluorogenic substrate 4MU-$GlcNAc_3$. Standard reaction mixtures contained 5 nM *Sc*CTS1, 0.1 mg/ml BSA, and 25–800 μM fluorogenic substrate in McIlvaine's buffer (100 mM citric acid, 200 mM sodium phosphate [pH 5.5]) to a final volume of 50 μl. Reaction mixtures were incubated for 30 min at 37°C, after which the reaction was stopped with the addition of 25 μl of 3 M glycine-NaOH (pH 10.3). The fluorescence of the released 4-methylumbelliferone was quantified using an Flx 800 microtiterplate fluorescence reader (Bio-Tek Instruments Inc) (excitation 360 nm, emission 460 nm). The standard used was 4-methylumbelliferone at a concentration range covering those of the substrate used in the kinetic experiments. Experiments were performed in triplicate. Production of 4-methylumbelliferone was linear with time for the incubation period used, and less than 10% of available substrate was hydrolyzed. The pH study was carried out with a mix of citric acid and sodium phosphate (McIlvaine's buffer system, pH from 2.2 to 7), and the assay was done under the same conditions as described above. The backgrounds were determined with all the components of the assay and at each individual concentration of the substrate without the enzyme. The backgrounds ranged from 1,100 to 1,600 fluorescence units and were used to correct the values obtained when the enzyme was present (fluorescence units up to 45,000). The stability of the enzyme at different pHs and concentrations of substrates was also verified. The enzyme behaved with a very similar activity (from pH 2.2 to 5) during a time-course incubation (up to 25 hr), showing that the pH did not affect the stability of the enzyme. To check for linearity of the enzyme at different pH, a continuous assay was established (same conditions but without stopping the reaction) at pH 2.2, 2.6, 3.0, 4.0, 5.0, 6.0, and 7.0, and the reaction followed for up to 5 hr. From these experiments, appropriate reaction times were selected for the stopped, steady-state kinetics assays, such that the reactions did not consume more than 10% of available substrate.

The same assay was used for screening The Prestwick Chemical Library (a library of 880 drug-like molecules obtained from Prestwick Chemical, Inc.). The inhibitors were screened at 40 μg/ml (approximately equivalent to 80 μM, assuming a molecular weight of 500) using a 4MU-$GlcNAc_3$ (substrate) concentration of 100 μM.

The IC_{50}s of allosamidin, kinetin, acetazolamide, and 8-chlorotheophylline were determined using the same protocol but with a constant substrate concentration of 100 μM, 0.1–50 μM allosamidin, 1–500 μM kinetin or acetazolamide, and 0.1–6 mM 8-chlorotheophylline. In order to check for potential irreversibility or tight binding character of kinetin, a continuous assay was followed for 5 hr, revealing that the activity was linear in absence or presence of 50 or 100 μM kinetin. Lineweaver-Burk analyses of steady-state kinetics with 50–500 μM of substrate in the presence of different concentrations of kinetin/acetazolamide were used to show that these molecules were competitive inhibitors.

Crystallization and Structure Determination

The protein was spin-concentrated up to 11.5 mg/ml. Crystals were grown by sitting drop experiments at 20°C by mixing 1 μl of protein with an equal volume of a reservoir solution (0.1 M HEPES, 0.8 M monosodium di-hydrogen phosphate, and 0.8 M monopotassium dihydrogen phosphate [pH 7.5]). The crystals under these conditions appeared within 5–9 days. For flash cooling, 0.1 M HEPES and 30% glycerol (pH 7.5) was used for native crystals prior to data collection.

For the *Sc*CTS1-inhibitor complexes, native crystals were soaked with either 8-chlorotheophylline (30 mM), acetazolamide (30 mM), or kinetin (saturated solution) for more than 30 min. These crystals were soaked with 0.1 M HEPES, 40% PEG 600 (pH 7.5) for 10 s and flash cooled with liquid nitrogen for storage and transfer to the synchrotron. Data were collected at the European Synchrotron Radiation Facility

(Grenoble, France). Diffraction data were processed with the HKL suite [35] (Table 1).

The native *Sc*CTS1 structure was solved by molecular replacement with MOLREP [36] using hevamine (PDB code 2HVM [3]) as a search model, giving a single solution with one molecule in the asymmetric unit. The resulting electron density map was of very good quality, allowing ARP/WARP to automatically build 270 out of 294 residues of the polypeptide chain. Further refinement (with REFMAC5 [37]) and model building (with COOT [38]) yielded a model with the final statistics shown in Table 1.

Refinement of *Sc*CTS1 complexed with 8-chlorotheophylline, kinetin and acetazolamide was initiated by rigid-body refinement, followed by simulated annealing with CNS [39] (for 8-chlorotheophylline) and iterative cycles of refinement and model building. Models for ligands were not included until their conformations were completely defined by unbiased $|F_o| - |F_c|$, f_{calc} electron density maps (Figures 4 and 5). Ligand starting structures and topologies were generated with PRODRG [40]. Further refinement resulted in the final models described in Table 1. WHAT IF [41] was used to calculate hydrogen bonds, and PyMol [42] was used to generate pictures.

ACKNOWLEDGMENTS

We thank the European Synchrotron Radiation Facility, Grenoble, for beam time. This work was supported by a Wellcome Trust Senior Research Fellowship and Project Grant, and the European Union FP6 STREP Fungwall program.

Received: September 28, 2006
Revised: February 16, 2007
Accepted: March 14, 2007
Published: May 29, 2007

REFERENCES

1. Adams, D.J. (2004). Fungal cell wall chitinases and glucanases. Microbiology *150*, 2029–2035.
2. Coutinho, P.M., and Henrissat, B. (1999). Carbohydrate-active enzymes: an integrated database approach. In Recent Advances in Carbohydrate Bioengineering, H.J. Gilbert, G. Davies, B. Henrissat, and B. Svensson, eds. (Cambridge, UK: The Royal Society of Chemistry), pp. 3–12.
3. Terwisscha van Scheltinga, A.C., Kalk, K.H., Beintema, J.J., and Dijkstra, B.W. (1994). Crystal-structures of hevamine, a plant defense protein with chitinase and lysozyme activity, and its complex with an inhibitor. Structure *2*, 1181–1189.
4. Bokma, E., Barends, T., Terwisscha van Scheltinga, A.C., Dijkstra, B.W., and Beintema, J.J. (2000). Enzyme kinetics of hevamine, a chitinase from the rubber tree *Hevea brasiliensis*. FEBS Lett. *478*, 119–122.
5. Bokma, E., Rozeboom, H.J., Sibbald, M., Dijkstra, B.W., and Beintema, J.J. (2002). Expression and characterization of active site mutants of hevamine, a chitinase from the rubber tree *Hevea brasiliensis*. Eur. J. Biochem. *269*, 893–901.
6. Brurberg, M.B., Nes, I.F., and Eijsink, V.G.H. (1996). Comparative studies of chitinases A and B from *Serratia marcescens*. Microbiology *142*, 1581–1589.
7. Correa, J.U., Elango, N., Polacheck, I., and Cabib, E. (1982). Endochitinase, a mannan-associated enzyme from *Saccharomyces cerevisiae*. J. Biol. Chem. *257*, 1392–1397.
8. Cabib, E., Roh, D.H., Schmidt, M., Crotti, L.B., and Varma, A. (2001). The yeast cell wall and septum as paradigms of cell growth and morphogenesis. J. Biol. Chem. *276*, 19679–19682.
9. Taib, M., Pinney, J.W., Westhead, D.R., McDowall, K.J., and Adams, D.J. (2005). Differential expression and extent of fungal/plant and fungal/bacterial chitinases of *Aspergillus fumigatus*. Arch. Microbiol. *184*, 78–81.
10. Dunkler, A., Walther, A., Specht, C.A., and Wendland, J. (2005). *Candida albicans* CHT3 encodes the functional homolog of the Cts1 chitinase of *Saccharomyces cerevisiae*. Fungal Genet. Biol. *42*, 935–947.
11. Perrakis, A., Tews, I., Dauter, Z., Oppenheim, A.B., Chet, I., Wilson, K.S., and Vorgias, C.E. (1994). Crystal structure of a bacterial chitinase at 2.3 Å resolution. Structure *2*, 1169–1180.
12. van Aalten, D.M.F., Synstad, B., Brurberg, M.B., Hough, E., Riise, B.W., Eijsink, V.G.H., and Wierenga, R.K. (2000). Structure of a two-domain chitotriosidase from *Serratia marcescens* at 1.9 Å resolution. Proc. Natl. Acad. Sci. USA *97*, 5842–5847.
13. Hollis, T., Monzingo, A.F., Bortone, K., Ernst, S., Cox, R., and Robertus, J.D. (2000). The X-ray structure of a chitinase from the pathogenic fungus *Coccidioides immitis*. Protein Sci. *9*, 544–551.
14. Rao, F.V., Houston, D.R., Boot, R.G., Aerts, J.M.F.G., Hodkinson, M., Adams, D.J., Shiomi, K., Omura, S., and van Aalten, D.M.F. (2005). Specificity and affinity of natural product cyclopentapeptide inhibitors against *Aspergillus fumigatus*, human and bacterial chitinases. Chem. Biol. *12*, 65–76.
15. Fusetti, F., von Moeller, H., Houston, D., Rozeboom, H.J., Dijkstra, B.W., Boot, R.G., Aerts, J.M.F.G., and van Aalten, D.M.F. (2002). Structure of human chitotriosidase—implications for specific inhibitor design and function of mammalian chitinase-like lectins. J. Biol. Chem. *277*, 25537–25544.
16. Reichard, U., Hung, C.-Y., Thomas, P.W., and Cole, G.T. (2000). Disruption of the gene which encodes a serodiagnostic antigen and chitinase of the human fungal pathogen *Coccidioides immitis*. Infect. Immun. *68*, 5830–5838.
17. Jaques, A., Fukamizo, K., Hall, T.D., Barton, R.C., Escott, G.M., Parkinson, T.C., Hitchcock, A., and Adams, D.J. (2003). Disruption of the gene encoding the ChiB1 chitinase of *Aspergillus fumigatus* and characterization of a recombinant gene product. Microbiology *149*, 2931–2939.
18. Kuranda, M.J., and Robbins, P.W. (1991). Chitinase is required for cell-separation during growth of *Saccharomyces cerevisiae*. J. Biol. Chem. *266*, 19758–19767.
19. Sakuda, S., Isogai, A., Matsumoto, S., Suzuki, A., and Koseki, K. (1986). The structure of allosamidin, a novel insect chitinase inhibitor produced by *Streptomyces sp*. Tetrahedron Lett. *27*, 2475–2478.
20. Sakuda, S., Nmoto, Y., Ohi, M., Watanabe, M., Takayama, S., Isogai, A., and Yamada, Y. (1990). Effects of demethylallosamidin, a potent yeast chitinase inhibitor, on the cell-division of yeast. Agric. Biol. Chem. *54*, 1333–1335.
21. Takaya, N., Yamazaki, D., Horiuchi, H., Ohta, A., and Takagi, M. (1998). Cloning and characterisation of a chitinase-encoding gene chiA from *Aspergillus nidulans*, disruption of which decreases germination frequency and hyphal growth. Biosci. Biotechnol. Biochem. *62*, 60–65.
22. Klemsdal, S.S., Clarke, J.H.L., Hoell, I.A., Eijsink, V.G.H., and Brurberg, M.B. (2006). Molecular cloning, characterization, and expression studies of a novel chitinase gene (ech30) from the mycoparasite *Trichoderma atroviride* strain P1. FEMS Microbiol. Lett. *256*, 282–289.
23. Terwisscha van Scheltinga, A.C., Armand, S., Kalk, K.H., Isogai, A., Henrissat, B., and Dijkstra, B.W. (1995). Stereochemistry of chitin hydrolysis by a plant chitinase/lysozyme and X-ray structure of a complex with allosamidin. Biochemistry *34*, 15619–15623.
24. Tews, I., Terwisscha van Scheltinga, A.C., Perrakis, A., Wilson, K.S., and Dijkstra, B.W. (1997). Substrate-assisted catalysis unifies two families of chitinolytic enzymes. J. Am. Chem. Soc. *119*, 7954–7959.

25. Sakuda, S., Isogai, A., Matsumoto, S., and Suzuki, A. (1987). Search for microbial insect growth-regulators. 2. Allosamidin, a novel insect chitinase inhibitor. J. Antibiot. (Tokyo) *40*, 296–300.

26. Walden, H., Bell, G.S., Russell, R.J.M., Siebers, B., Hensel, R., and Taylor, G.L. (2001). Tiny TIM: a small, tetrameric, hyperthermostable triosephosphate isomerase. J. Mol. Biol. *306*, 745–757.

27. van Aalten, D.M.F., Komander, D., Synstad, B., Gåseidnes, S., Peter, M.G., and Eijsink, V.G.H. (2001). Structural insights into the catalytic mechanism of a family 18 exo-chitinase. Proc. Natl. Acad. Sci. USA *98*, 8979–8984.

28. Papanikolau, Y., Prag, G., Tavlas, G., Vorgias, C.E., Oppenheim, A.B., and Petratos, K. (2001). High resolution structural analyses of mutant chitinase A complexes with substrates provide new insight into the mechanism of catalysis. Biochemistry *40*, 11338–11343.

29. Boot, R.G., Blommaart, E.F., Swart, E., Ghauharali-van der Vlugt, K., Bijl, N., Moe, C., Place, A., and Aerts, J.M. (2001). Identification of a novel acidic mammalian chitinase distinct from chitotriosidase. J. Biol. Chem. *276*, 6770–6778.

30. Synstad, B., Gaseidnes, S., van Aalten, D.M.F., Vriend, G., Nielsen, J.E., and Eijsink, V.G.H. (2004). Mutational and computational analysis of the role of conserved residues in the active site of a family 18 chitinase. Eur. J. Biochem. *271*, 253–262.

31. Rao, F.V., Houston, D.R., Boot, R.G., Aerts, J.M., Sakuda, S., and van Aalten, D.M.F. (2003). Crystal structures of allosamidin derivatives in complex with human macrophage chitinase. J. Biol. Chem. *278*, 20110–20116.

32. Berecibar, A., Grandjean, C., and Siriwardena, A. (1999). Synthesis and biological activity of natural aminocyclopentitol glycosidase inhibitors: mannostatins, trehazolin, allosamidins and their analogues. Chem. Rev. *99*, 779–844.

33. Rao, F.V., Andersen, O.A., Vora, K.A., DeMartino, J.A., and van Aalten, D.M.F. (2005). Methylxanthine drugs are chitinase inhibitors: investigation of inhibition and binding modes. Chem. Biol. *12*, 973–980.

34. Schuettelkopf, A.W., Andersen, O.A., Rao, F.V., Allwood, M., Lloyd, C., Eggleston, I.M., and van Aalten, D.M.F. (2006). Screening-based discovery and structural dissection of a novel family 18 chitinase inhibitor. J. Biol. Chem. *281*, 27278–27285.

35. Otwinowski, Z., and Minor, W. (1997). Processing of X-ray diffraction data collected in oscillation mode. Methods Enzymol. *276*, 307–326.

36. Vagin, A., and Teplyakov, A. (1997). MOLREP: an automated program for molecular replacement. J. Appl. Cryst. *30*, 1022–1025.

37. Murshudov, G.N., Vagin, A.A., and Dodson, E.J. (1997). Refinement of macromolecular structures by the maximum-likelihood method. Acta Crystallogr. D Biol. Crystallogr. *53*, 240–255.

38. Emsley, P., and Cowtan, K. (2004). Coot: model-building tools for molecular graphics. Acta Crystallogr. D Biol. Crystallogr. *60*, 2126–2132.

39. Brunger, A.T., Adams, P.D., Clore, G.M., Gros, P., Grosse-Kunstleve, R.W., Jiang, J.-S., Kuszewski, J., Nilges, M., Pannu, N.S., Read, R.J., et al. (1998). Crystallography and NMR system: a new software system for macromolecular structure determination. Acta Crystallogr. D Biol. Crystallogr. *54*, 905–921.

40. Schuettelkopf, A.W., and van Aalten, D.M.F. (2004). PRODRG: a tool for high-throughput crystallography of protein-ligand complexes. Acta Crystallogr. D Biol. Crystallogr. *60*, 1355–1363.

41. Vriend, G. (1990). WHAT IF: a molecular modeling and drug design program. J. Mol. Graph. *8*, 52–56.

42. DeLano, W.L. (2004). The PyMOL Molecular Graphics System (http://www.pymol.org).

Accession Numbers

The coordinates and structure factors have been deposited with the following PDB codes (entries 2UY2, 2UY3, 2UY4, and 2UY5).